Coastal Dynamics 2017
Paper No. 025

CRESCENTIC BAR PATTERNS ALONG CURVED COASTS: OBSERVATIONS AND MODELLING

Jantien Rutten[1], Benjamin Dubarbier[2], Timothy Price[1], Bruno Castelle[2] and Gerben Ruessink[1]

Abstract

Characteristic crescentic sandbar patterns, with alternating landward and seaward protrusions, are relatively well-studied along straight coasts. However, along curved coasts, where wave characteristics vary alongshore due to the varying coastline orientation, patterning is poorly understood. Here, we aim to determine the alongshore variation in crescentic pattern formation and the associated wave forcing along curved coasts, using a 2.4-year video dataset of the Sand Engine and a non-linear morphodynamic model. Our observations indicate that patterning varied alongshore, and is related to the local wave angle. Consistent with studies on straight coasts, both our observations and modelling results indicate that pattern formation is stimulated by near-normal waves, but inhibited by oblique waves. Moreover, time-varying angles further affect alongshore differences in crescentic patterning.

Key words: sandbars, pattern formation, convex coastline, morphodynamics, video imagery, numerical modelling

1. Introduction

Sandbars, submerged ridges of sand parallel to the shore, tend to develop an alongshore variability in depth and position, while migrating onshore (Wright and Short, 1984). Characteristic crescentic patterns, with shallow landward protruding horns and deeper seaward protruding bays, have been observed to develop in initially alongshore-uniform bars along many wave-dominated sandy beaches (Sonu, 1973; Wright and Short, 1984; Lippmann and Holman, 1990; Van Enckevort and Ruessink, 2003). Alongshore length scales of these patterns are *O*(100-1000 m), while cross-shore amplitudes are *O*(10 m) (Van Enckevort et al., 2004). Typical wave conditions associated with the formation of crescentic patterns are low-energetic (Wright and Short, 1984). In addition, several modelling studies show that shore-normal wave incidence stimulates pattern formation (e.g. Calvete et al., 2005; Drønen and Deigaard, 2007; Splinter et al., 2011). Under such conditions, small-scale irregularities self-organize into larger scale patterns, through positive feedback between flow and morphology (Falqués et al., 2000).

Although many beaches worldwide have a certain curvature, most studies on crescentic patterns focused on straight coastlines, neglecting any influence of coastline curvature on both the occurrence and formation of patterning. A curved coast imposes an alongshore variation in local wave characteristics, such as wave angle and breaker height, through its varying coastline orientation. This may importantly affect bar response on a local scale and thus induce a spatial variability in bar morphology and its behaviour. For example, sandbars along embayed beaches have been found to rotate with respect to the mean bar crest position due to a spatial variation in cross-shore migration rate (Blossier et al., 2016; Ojeda et al., 2011). Also, alongshore variation in alongshore variability has been found along curved embayed beaches, by morphodynamic modelling (Castelle and Coco, 2012) and from observations at several coasts, such as Fisherman's-Collaroy-Narrabeen, Australia (Wright and Short, 1984), and Monterey Bay, U.S.A. (Thornton et al., 2007). Moreover, observations at the convex, man-made curved coast of the Sand Engine, The Netherlands, suggest the importance of coastline curvature on spatiotemporal variability in crescentic pattern formation (Rutten et al., 2017). Here, patterns have been observed either at the western side, or at

[1]Dept. Physical Geography, Faculty of Geosciences, Utrecht University, The Netherlands. j.rutten@uu.nl, t.d.price@uu.nl, and b.g.ruessink@uu.nl
[2]UMR CNRS 5805 EPOC, OASU, University of Bordeaux, France, benjamin.dubarbier@u-bordeaux.fr, b.castelle@epoc.u-bordeaux1.fr

the northern side, at both sides, or were entirely absent (Figure 1). The wave conditions and underlying mechanisms related to alongshore differences in crescentic pattern formation along curved coasts are, however, not well understood. Given the recent trend in coastal policy to the construction of large-scale $O(10\ \mathrm{Mm}^3)$ coastline perturbations that protect on decadal timescales (Stive et al., 2013), better insight is required how curved coasts affect the nearshore zone. Here, we aim to determine the wave conditions related to crescentic pattern formation and its alongshore variability, along curved coasts. We use a 2.4-year Argus video data set (Holman and Stanley, 2007) of the Sand Engine, and a process-based morphodynamic model. In Section 2, we introduce the field site, and the data set consisting of video observations and wave buoy measurements. Then, we describe crescentic pattern formation at the Sand Engine, and determine the wave conditions associated with them. Section 3 introduces the model and our model set-up. Section 4 describes our model results and how modelled bar patterns compare to observations at the Sand Engine. Finally, Section 5 discusses the driving mechanisms and future work, and in Section 6 the main conclusions are presented.

2. Motivation: observations at the Sand Engine

2.1 The Sand Engine

The Sand Engine, a 21.5 Mm^3 nourishment constructed in July 2011 as long-term and environmentally-friendly measure against coastal erosion, creates locally a strong curvature in the coastline of the Delfland coast, The Netherlands (Figure 2). Its cross- and alongshore dimensions change in time, i.e. erosion at the Sand Engine's tip and growth at the adjacent beaches. This feeder effect, intended for supplying the adjacent beaches gradually with sand for several decades, arises by gradients in the alongshore sediment transport that are induced by the curved coast and the prevailing wave climate, and is also referred to as diffusion. To illustrate, De Schipper et al. (2016) show from a bathymetric data set that the nourishment itself lost 1.5 Mm^3 in 1.5 year, while the adjacent beaches northwest and southeast of the nourishment gained 0.7 and 0.5 Mm^3, respectively. Numerical predictions by Arriaga et al. (2017) confirm the diffusive behaviour of the Sand Engine on the long-term, e.g. a reduction in cross-shore amplitude from 950 m in 2012 to 450 m in 2025. Consequently, the curvature will decrease, and thereby the alongshore variation in coastline orientation.

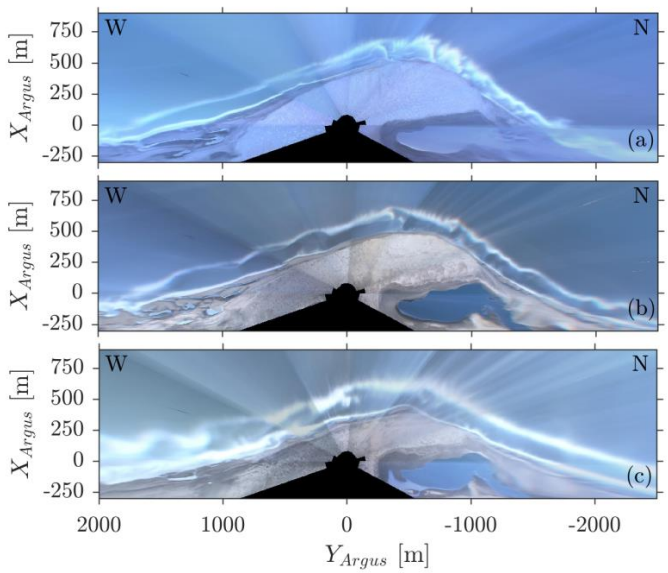

Figure 1. Examples of ten-minute averaged planview images on (a) 4 June 2013, (b) 23 November 2013, and (c) 24 January 2015 at the Sand Engine. The white elongated lines indicate the time-averaged position of wave breaking, which approximate the location of the sandbar (outer breaker line) and shoreline (inner breaker line). Alongshore differences in crescentic patterning can be observed that change in time.

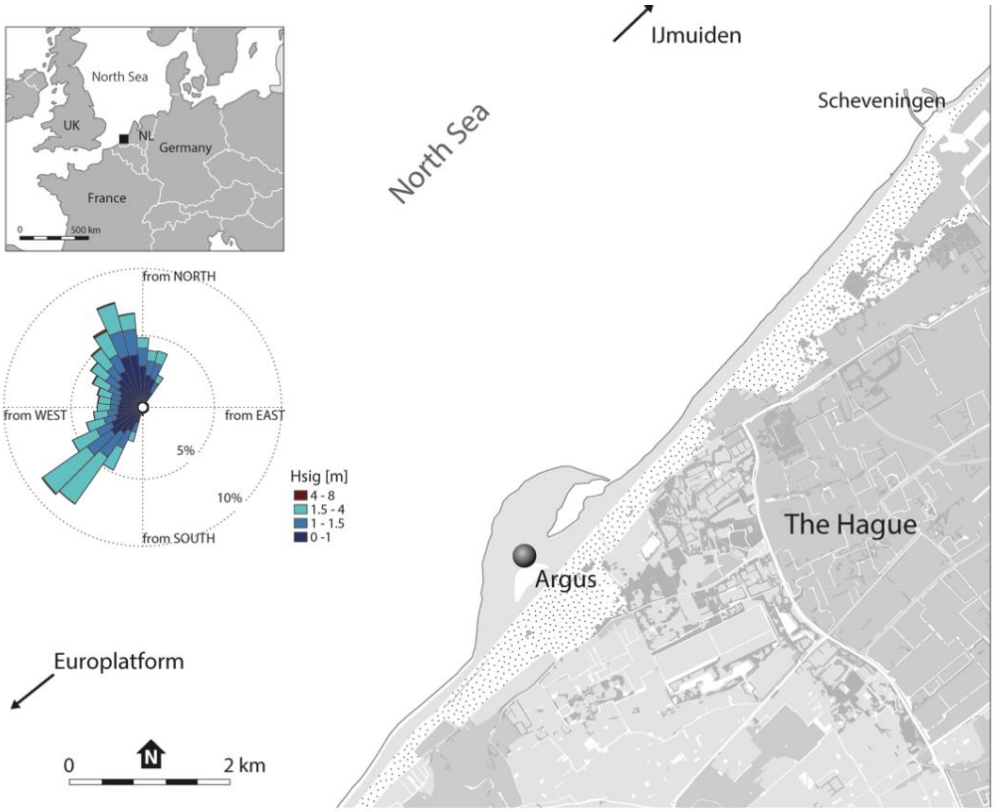

Figure 2. Location of Sand Engine, The Netherlands; and wave rose showing significant wave height H_{sig} and direction in 2005-2015, measured at 32 m depth at the Europlatform. Beach (gray shading), dune area (dots), and built-up area (different gray tints) are indicated.

The Sand Engine, located along the north-easterly (42° from the north) oriented Delfland coast is exposed to a bimodal wave climate with waves from the north-northwest (347° N; Figure 2) and southwest (222° N). The yearly-averaged significant wave height H_{m0} is 1.3 m, with a corresponding peak period T_p of 5.7 s. The wave climate possesses certain seasonality with low to moderately energetic waves (H_{m0} = 1.1 m) dominating spring and summer (April-September), while autumn and winter (October-March) are characterized by storms (H_{m0} up to 5 m, T_p up to 9 s) that pass from southwest to northwest. The tide is semi-diurnal with a mean tidal range of 1.7 m, and alongshore velocities up to 0.5 m/s. The sand at the Sand Engine has a mean grain diameter D_{50} of 280 µm (De Schipper et al., 2016).

2.2 Video data set

A 2.4-year data set of daily video images was collected in March 2013-July 2015 by an Argus video station consisting of eight 5.0 Mega Pixel cameras atop a tower at 42.7 m + MSL (Mean Sea Level; N 52.05083° E 4.18447°). Ten-minute averaged images were used, as they reveal white elongated lines, indicating the time-averaged position of wave breaking, that serve as proxies for the positions of the sandbar and shoreline (Lippmann and Holman, 1989; Van Enckevort and Ruessink, 2001; Figure 1). Several pre-processing steps were required. First, each camera was calibrated for lens distortion in the laboratory. Second, the 2048 × 2448 pixels in the eight individual images were projected on a horizontal plane and merged. More specifically, pixel coordinates were transformed to world coordinates (x,y,z), via two photogrammetric equations (Holland et al., 1997) wherein z was assumed constant at the tidal level. The equations were solved for each camera using camera-specific parameters, i.e. position (x_0,y_0,z_0), orientation (pitch, roll, azimuth), field of view, and focal length. The orientation of each camera was calculated from Ground Control Points (GCPs), reference points within the field of view of the corresponding camera whereof world coordinates are known. Temporary GCPs, obtained by a car equipped with a dGPS system,

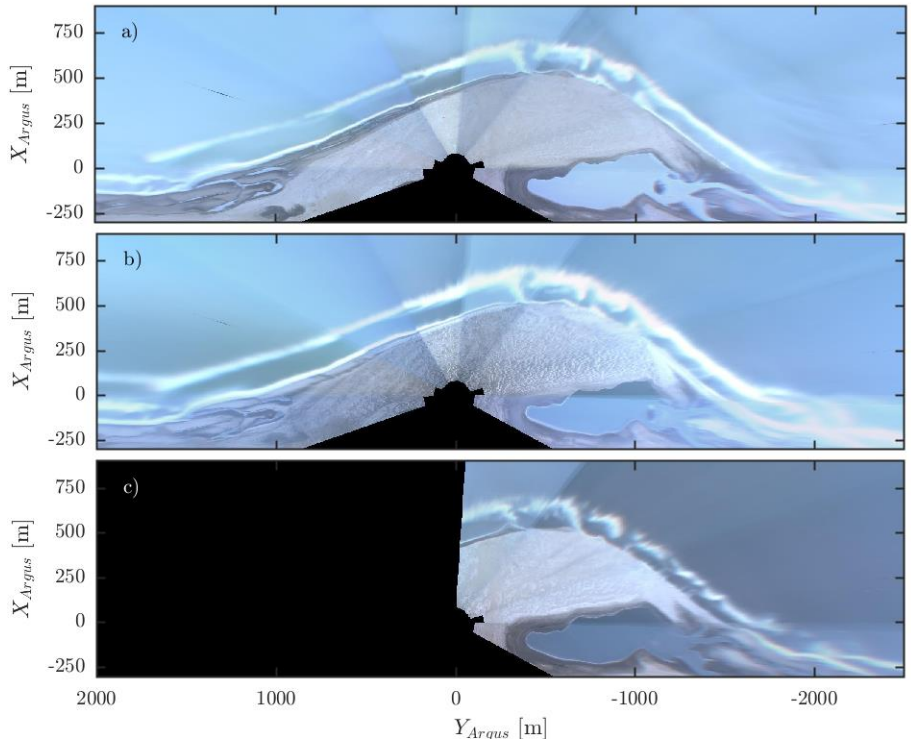

Figure 3. Sequence of video images, showing an example of pattern formation at the northern side (-1500 < Y_{Argus}< -900 m), under nearly constant wave angle, on (a) 2 March, (b) 10 March, and (c) 3 April 2013. Waves approached shore-normal at the northern side.

were used to deduce initial camera orientations. Virtual GCPs were used to correct for minute changes in camera orientation over time, due to e.g. winds or thermal expansion. Such slight changes may lead to changes in the area observed by the camera and therefore the geo-referencing of pixels to world coordinates will no longer be accurate. We used beach poles visible in the images, as virtual GCPs, as well as the horizon, to geo-reference accurately the 2.4-year data set. Unfortunately, the required minimum of two GCPs, in addition to the horizon, was not fulfilled for camera 5 and 6.

Resulting plan view images have their own local coordinate system, with the origin located at the Argus tower, the *y*-axis, aligned with the regional coastline, positive to the SW (220° N), and the *x*-axis positive offshore. They cover 4500 m in the alongshore direction, and 1200 m in the cross-shore direction, with a grid resolution of 2 m. The data set consists of 778 images that are recorded at low tide, to eliminate tide-induced variability in breaker line position. Low tides were found to give the clearest breaker line patterns. Some days, no images with breaker patterns were available, e.g. due to low energetic days without wave breaking, fog, or camera failure.

2.3 Observations on crescentic patterning

Our video observations reveal a spatiotemporal variability in crescentic patterning along the curved coast of the Sand Engine (Figure 1). Generally, patterns at the northern side were observed to develop gradually in spring and summer, when waves of moderate height (H_{m0} =0.5-1.5 m, at 10 m depth) approached from the north-northwest for several weeks. At the same time, the bar at the western side remained straight. An example hereof is shown in Figure 3. Due to the curved coast, local incidence angles were shore-normal at the northern side and highly oblique at the western side. Such crescentic patterns were partly or fully smoothed out in a few days during either a single or series of autumn storms with peaks in H_{m0} of 1-3 m.

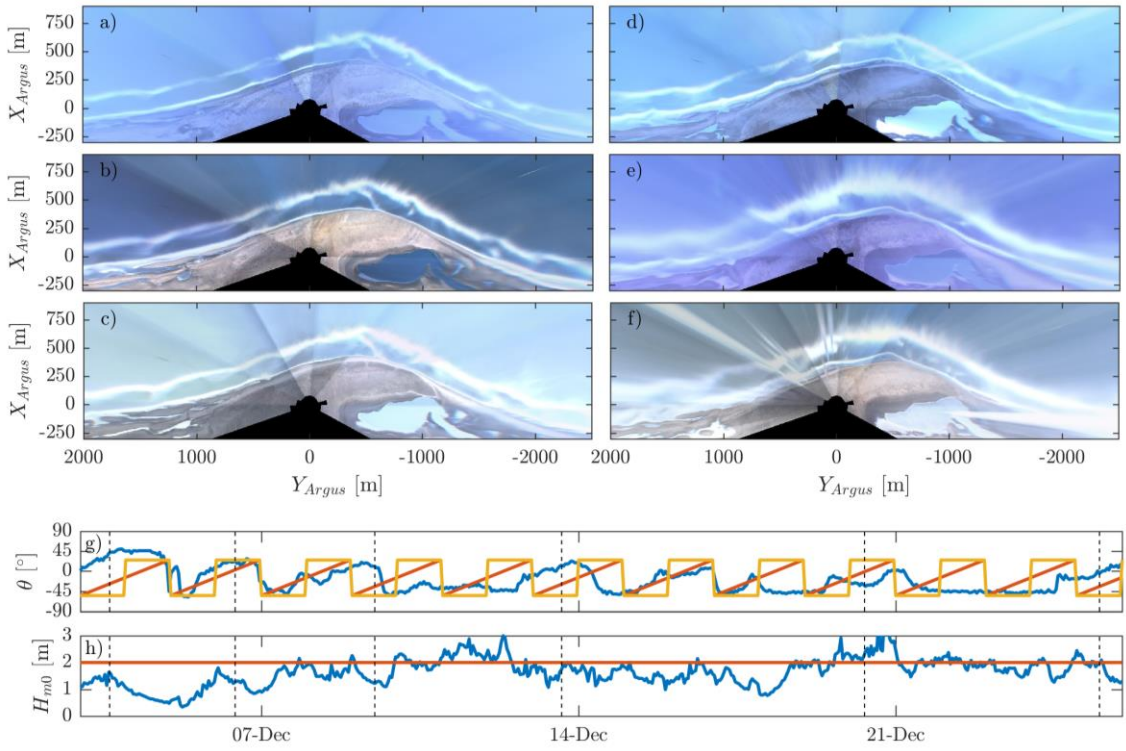

Figure 4. Sequence of video images, showing an example of crescentic pattern formation at the western side (-200 < Y_{Argus}<2000 m) under a series of storms with time-varying wave angle, on (a) 3 December, (b) 6 December, (c) 9 December, (d) 13 December, (e) 20 December, and (f) 25 December 2014. Measured (g) wave angle θ and (h) significant wave height H_{m0} at 10 m depth are indicated in blue, whereas yellow (g) and red (g,h) show forcing for different model scenarios. Zero θ coincides with the shore-normal of the regional coastline, positive/negative is to the north/south. Vertical dashed lines (in g,h) indicate the dates of the images.

These conditions, in contrast, stimulated pattern formation at the western side. More in detail, Figure 4 shows how patterns developed in the alongshore-uniform sandbar at the western side within several weeks under a series of storms, while the sandbar at the northern side remained straight. At the Delfland coast, storms typically have a time-varying wave angle, since they pass from southwest to northwest through the North Sea basin, and thus incidence angles are weakly oblique at the western side but highly oblique at the northern side of the Sand Engine. Figure 4g shows that the storms varied in wave angle θ, i.e. its time evolution and thus predominant direction of each storm. For example, the storm on 9-13 December is energetic from the west (θ = 273°) for ~3 days, but subsides when turning to the north-northwest (θ = 335°). In contrast, the storm on 19-21 December rises when turning from west (θ = 267°) to west-northwest (θ = 290°) to northwest (θ = 315°). Thus, our field observations indicate the importance of θ on pattern formation along a curved coast, for further details see Rutten et al. (2017). However, our data set cannot explain the underlying processes behind the observed formation of crescentic patterns. Therefore, we continue with a numerical model, and systematically test time-invariant and time-varying angles along a barred curved coast.

3. Model

3.1 Model description

We use a non-linear, depth-averaged morphodynamic model (Dubarbier et al., in revision). Both cross-shore and alongshore processes are in such a way included that bars can migrate in the cross-shore direction, but also develop certain alongshore variability in position and depth. Here, we focus on the

growth and evolution of crescentic patterns only. We refer to Dubarbier et al. (in revision) for simulations of the full accretionary downstate evolution of a barred beach along a straight coast.

The model consists of four modules. First, the wave field is computed with the spectral wave model SWAN v41.10 (Booij et al., 1999), which solves the wave action balance. Second, the horizontal flow field is computed via the time- and depth-averaged non-linear shallow water equations, and includes the wave return flow (undertow). The time-averaging operator is sufficiently small to handle variations due to tides and varying wave regimes, but too high to explicitly simulate infra-gravity motions. Third, the total sediment transport Q_t is obtained with an energetics-type sediment transport equation, based on Hsu et al. (2006) and Dubarbier et al. (2015), and consists of three modes of sediment transport, reading as

$$Q_t = Q_w + Q_c - Q_d \tag{1}$$

with transports related to orbital velocity skewness Q_w, wave-induced mean current Q_c, and gravitational downslope effects Q_d. Individual transports contain both bed load and suspended load. Fourth, the bed level is updated trough the sediment mass conservation equation. For further detail on the four modules, we refer to Dubarbier et al. (in revision).

Within the sediment module, we used a mean grain diameter d_{50} of 290 µm, and adjusted the coefficients C_w, C_c and C_f that scale the contribution of each corresponding transport – from 0.08 (default) to 0.02, 0.04, and 0.08, respectively. New coefficients were determined in a sensitivity analysis, wherein C_w:C_C = 0.02:0.04 allowed the bar to migrate onshore and meanwhile develop alongshore variability similar to the observations at the Sand Engine. The relatively high coefficient of diffusive transport C_f was needed to smooth unrealistic steepening of the bar and beach face, and to prevent consequent crashes of the simulations.

3.2 Model set-up and scenarios

To systematically test the influence of wave forcing on crescentic bar behaviour along curved coasts, we adopted an idealized approach. A synthetic bathymetry was created in several steps, based on bathymetric measurements at the Sand Engine in November 2014 when the bar at its west side was alongshore-uniform (Figure 5a). First, a curved coastline was generated from the best fit of a Gaussian curve through the 0-contour line in the bathymetric measurements, wherein the Gaussian shape function reads as

$$x = p_1 + p_2 e^{\frac{-(y+p_3)^2}{2{p_4}^2}} \tag{2}$$

with cross-shore coordinate x, alongshore distance y and function coefficients p_1 = 253.36, p_2=-698.37, p_3=-494.33, and p_4 =-926.30. Second, a barred profile was created as the best fit of the double-slope profile function of Yu and Slinn (2003) with a 500 m alongshore average of the measured profile at the west side of the Sand Engine. The resulting profile function reads as

$$h = \left(x_s - \frac{x_s}{\gamma}\right)\frac{\tanh\tan\beta_1 x}{x_s} + \frac{\tan\beta_1 x}{\gamma} - b_h e^{-b_w}\left(\frac{x-x_c}{x_c}\right)^2 \tag{3}$$

with water depth h, and function coefficients $\gamma = \tan\beta_1/\tan\beta_2$, β_1 = 0.0372, β_2 = 0.0112, x_s = 3.626, x_c = -222.62, b_h = -2.389, and b_w = 11.07. Herein, the first and second term create a profile with slope β_1 in the upper part and slope β_2 in the lower part. The third term creates a perturbation, of amplitude b_h and width b_w, that resembling the sandbar. Third, the profile was rotated along the Gaussian-shaped coastline. Fourth, bed elevation was linearly interpolated to a rectangular grid with a resolution of 10 m, over 7000 m in the alongshore direction and 2600 m in the cross-shore direction. In the coordinate system the x-axis is positive onshore, as prescribed by the model, the y-axis is positive to the right, and the origin is similarly positioned as in the video observations. Fifth, the curvature of the perturbation in deeper depth contours was gradually reduced, as is also observed in the field (Figure 5a), by locally re-computing the profile and replacing bed elevations larger than -15 m by -15 m. More specifically, we interpolated linearly between -12 m and the offshore grid boundary. Sixth, millimetric random perturbations were added to the bathymetry to initiate pattern formation.

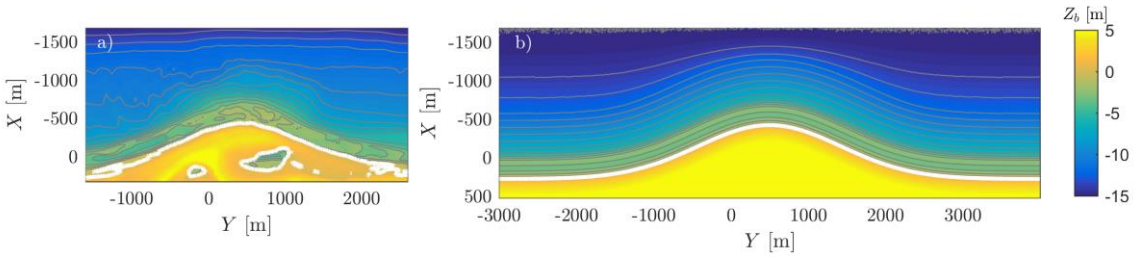

Figure 5 (a) Measured bathymetry at the Sand Engine in November 2014, and (b) synthetic bathymetry with alongshore-uniform bar, based on measurements in (a). Colours indicate bed elevation.

The synthetic bathymetry is exposed to a forcing with time-invariant and time-variant wave angle, which are schematizations of the conditions that drove crescentic pattern formation at the northern and western side of the Sand Engine, respectively. To reveal insight into the dependency of alongshore variability in pattern formation on a time-varying angle, two scenarios were tested that differed in the function of variation – abruptly and sawtooth (see Figure 4g). Herein, θ varied over two days from -55 to 25°, with $\theta = 0°$ shore-normal along the straight coastline and $\theta = 25°$ shore-normal along the right side of the perturbation. All three scenarios have a significant wave height H_s of 2 m, and a peak wave period T_p of 8 s, and were run over a period of 14 days with morphodynamic time step of 30 min (Table 1).

4. Model assessment on crescentic pattern formation

4.1 Time-invariant wave angle

Crescentic patterns developed along the right side of the perturbation and the straight adjacent coast (1400 < Y < 4000 m, -3000 < Y < -2000 m), when imposing a time-invariant wave forcing, H_s = 2.0 m, T_p = 8.0 s and $\theta = 25°$ (Table 1; Figure 6). Along the left side, no patterns developed. Initially the bar only migrated onshore, but after several days also certain alongshore variability can be distinguished in the sandbar at the right side (Figure 6a). Here, waves approached shore-normally (Figure 6a; white arrows), generating horizontal circulation cells in the flow field (Figure 6a; red arrows). Through positive feedback between morphology and flow, small irregularities grew into quasi-rhythmic patterns of O(100 m), of a similar order of magnitude as our observations of crescentic bars at the Sand Engine (Figure 3). In time, the characteristic lunate-shaped bars propagated onshore and became more pronounced, while the rip channels in-between deepened. At the left side, waves approached obliquely ($\theta_L = 50°$) and refracted considerably on the perturbed depth contours (Figure 6a; -2000 < Y < 0 m). This resulted in reduced incident wave energy and the generation of an alongshore current, which both may have prevented pattern formation at this side.

4.2 Time-varying wave angle

No patterns developed, when exposing the coast by a time-varying wave forcing, with θ shifting abruptly from -55 to 25° every day (H_s = 2.0 m, T_p = 8.0 s; Table 1; Figure 7a-c). At both the left and right side and along the straight coast, waves approached locally obliquely ($\theta_L = 50°$, $\theta_R = -80°$ and $\theta_S = -55°$) for one of the angles (θ = *-55* or *25*°) and refracted. Consequently, incident wave energy reduced and an alongshore current (Figure 7a-c; red arrows) was generated. In contrast, the observations of the Sand Engine do show pattern formation at the western side under such angles. The mismatch between model and observations may be due to the schematization of θ. Figure 4g shows that measured θ changed slightly gradual, and

Table 1. Applied wave forcing in simulations.

	H_s	T_p	θ	t
Run 1	2.0 m	8.0 s	25°	14 days
Run 2	2.0 m	8.0 s	-55, 25° (abrupt)	14 days
Run 3	2.0 m	8.0 s	-55, 25° (sawtooth)	14 days

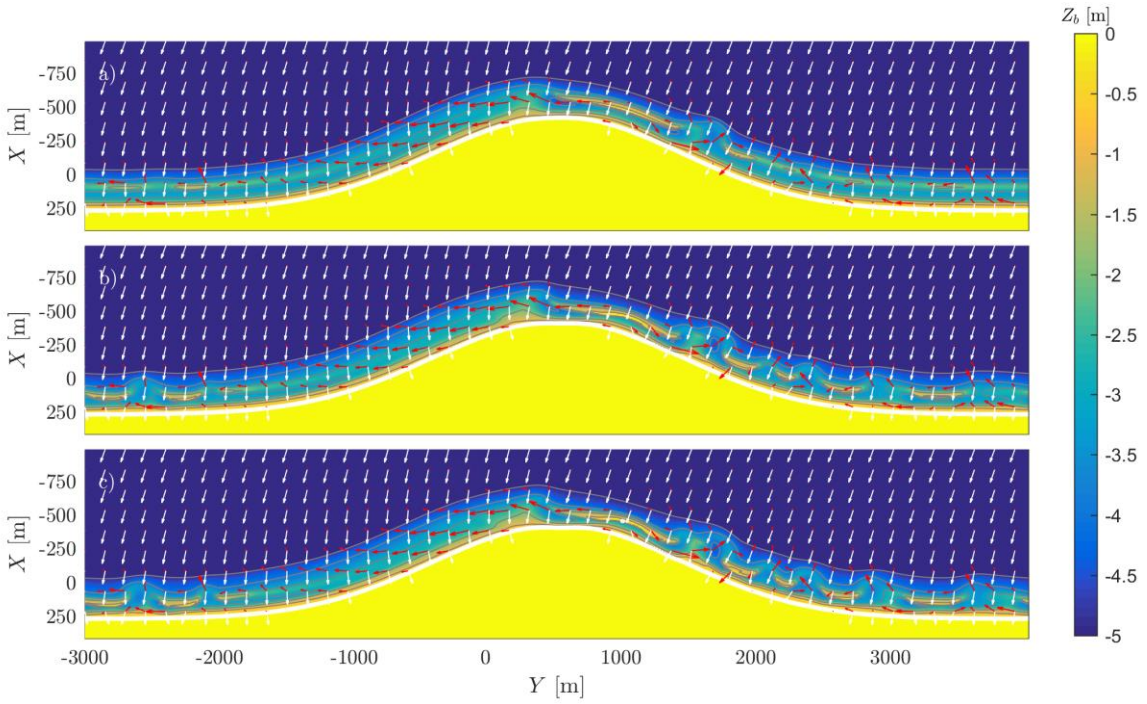

Figure 6. Simulated bed evolution after (a) 8 days, (b) 12 days, and (c) 14 days, for time-invariant wave forcing (H_s = 2.0m, T_p = 8.0s and θ=25°). Colours indicate bed elevation z_b, and arrows indicate θ (white) and current (red).

consequently the Sand Engine was exposed to smaller θ, in addition to θ= -55 and 25°. Indeed, when exposing the coast to a gradually shifting θ from -55 to 25° every day, using a sawtooth function (Figure 4g; red line), patterns developed at the left side of the perturbation and along the straight coast (Figure 7d-f; -3000 < Y < -300 m; 2700 < Y < 4000 m). Herein, the presence of patterns can be explained by the reduction of extreme θ within the scenario, thereby limiting refraction, energy losses, and alongshore currents. Although the gradual change of θ, and thus low obliquity, is overrepresented in this scenario (see Figure 4g), it clearly illustrates the negative effect of prolonging high incidence on pattern formation.

5. Discussion

Our model results show that oblique waves, i.e. θ > 50°, present at least half of the simulation time, prevent pattern formation within the 14-day simulation period. Potentially, patterns may develop for longer simulation periods. For example, Calvete et al. (2005) and Thiebot et al (2012) show that patterns can develop under oblique waves, but with lower growth rates. Garnier et al. (2009) show that the mechanism behind reduced growth rates was not directly related to alongshore currents but to a decrease in incoming wave energy due to refraction of the oblique waves. As a result, cell circulation was weaker for oblique incidence than shore-normal incidence, thereby reducing the growth rate of patterns. Garnier et al. (2009) tested the effect of obliquity only for θ = 4°. However, under higher obliquity, cell-circulation will become weaker and the strength of the alongshore current will increase. In these situations, the alongshore current might contribute directly in inhibiting pattern formation, but requires further research.

Figure 7 shows that different variations on a time-varying θ affect the alongshore patterning importantly. Castelle and Ruessink (2011) show crescentic pattern formation and their non-linear evolution for several variations on a time-varying wave θ along a straight coast. Consistent with our findings, they found reduced growth rates, and thus reduced pattern formation, for an abruptly changing θ compared to a gradually changing θ (e.g. sawtooth). How patterning along curved coasts is affected by different variations of a time-varying θ is unknown, both in terms of its function (e.g. abrupt, sawtooth, cosine) and its

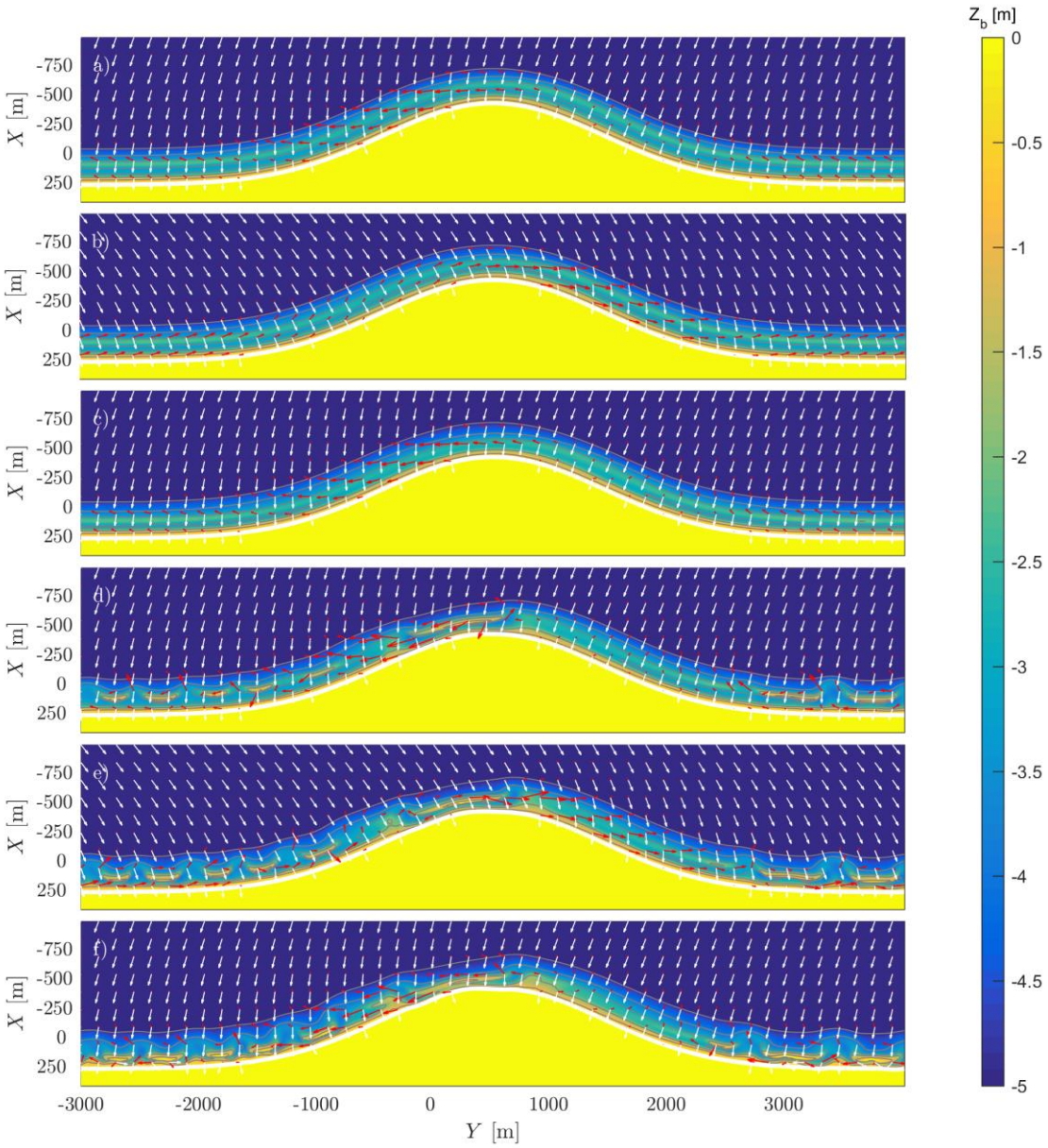

Figure 7. Simulated bed evolution after (a,d) 8 days, (b,e) 10 days, and (c,f) 14 days, for H_s = 2.0m, T_p = 8.0s, and shifting wave angle θ between -55 and -25° every day , (left column) abruptly, or (right column) sawtooth function (see Figure 4g, red and yellow angle). Colors indicate bed elevation z_b, and arrows indicate θ (white) and flow direction (red).

extremes (θ_1, θ_2). In addition, coasts with a stronger or weaker curvature may impose differences in crescentic patterning, since the curvature of the coast affects the local coastline orientation and thereby the local wave angle. Therefore, further study is required to get a more general understanding on crescentic patterning along curved coasts.

6. Conclusion

From observations at the Sand Engine, we may conclude that opposite effects in crescentic patterning at its northern and western side are related to the local wave angle, varying in time due to the bimodal wave climate and varying alongshore due to the changing coastline orientation of the curved coast. Under

prolonged periods of north-northwestern waves, patterns developed along the northern side where waves approached locally near-normal. Meanwhile, the bar along the western side remained straight. Under a series of storms approaching from southwest to northwest, patterns developed at the western side where waves approached locally weakly oblique. As the northern side was consequently exposed to highly oblique angles, no patterns developed here. Numerical tests on time-invariant and time-variant wave angles at a curved coast, using a non-linear morphodynamic model, resulted in crescentic patterns similar as observed at the Sand Engine, both with alongshore length scales of $O(100$ m). In line with our observations, crescentic patterns developed where waves approached locally near-normal, promoting horizontal cell-circulation that, via positive feedback between flow and morphology, drove crescentic patterning. The refraction of highly obliquely incident waves, however, reduced wave energy and drove an alongshore current, which may have prevented the development of patterns, also when high obliquity was present only half of the simulation period. Gradually varying wave angles, as opposed to abruptly varying ones, reduced the duration of high obliquity within our simulation, resulting in an increase of crescentic patterns.

Acknowledgements

Jantien Rutten and Gerben Ruessink were funded by the Dutch Technology Foundation STW that is part of the Dutch Organisation for Scientific Research (NWO), and which is partly funded by the Ministry of Economic Affairs, under contract 12686 (Nature Coast: S1 Coastal Safety). Timothy Price was funded by the Dutch Organisation for Scientific Research (NWO), under contract 016.Veni.171.101. Bruno Castelle and Benjamin Dubarbier were funded by the Agence Nationale de la Recherche (ANR) through project CHIPO (ANR-14-ASTR-0004-01). We thank Deltares for the acquisition of the Argus imagery, and SHORE Monitoring & Research for the collection of the bathymetric data at the Sand Engine.

References

Arriaga, A., Rutten, J., Ribas, F., Falqués, A., Ruessink, B.G., 2017. Modeling the long-term diffusion and feeding capability of a mega-nourishment. *Coastal Engineering* 121: 1-13.

Blossier, B., Bryan, K.R., Daly, C.J., Winter, C., 2016. Nearshore sandbar rotation at single-barred embayed beaches. *Journal of Geophysical Research: Oceans* 121, doi: 1.1002/2015JC011031.

Booij, N., Ris, R.C., Holthuijsen, L.H., 1999. A third-generation wave model for coastal regions 1. Model description and validation. *Journal of Geophysical Research* 104. No C4: 7649-7666.

Calvete, D., Dodd, N., Falqués, A., Van Leeuwen, S.M., 2005. Morphological development of rip channel systems: Normal and near-normal wave incidence. *Journal of Geophysical Research* 110. C10006, doi:10.1029/2004JC002803.

Castelle, B. and Ruessink, B.G., 2011. Modeling formation and subsequent nonlinear evolution of rip channels: Time-varying versus time-invariant wave forcing. *Journal of Geophysical Research* 116, F04008, doi:10.1029/2011JF001997.

Castelle, B., Coco, G., 2012. The morphodynamics of rip channels on embayed beaches. *Continental Shelf Research*, 43, 10-23.

Coco, G., Murray, A.B., 2007. Patterns in the sand: From forcing templates to self-organization. *Geomorphology* 91: 271-290.

De Schipper, M.A., De Vries, S., Ruessink, B.G., De Zeeuw, R.C., Rutten, J., Van Gelder-Maas, C., Stive, M.J.F., 2016. Initial spreading of a mega feeder nourishment: Observations of the Sand Engine pilot project. *Coastal Engineering* 111: 23-38.

Drønen, N., Deigaard, R., 2007. Quasi-three-dimensional modelling of the morphology of longshore bars. *Coastal Engineering* 54: 197-215.

Dubarbier, B., Castelle, B., Marieu, V., Ruessink, B.G., in revision. Mechanisms controlling the complete accretionary beach state sequence. *Geophysical Research Letters*. .

Dubarbier, B., Castelle, B. Marieu, V., Ruessink, B.G., 2015. Process-based modeling of cross-shore sandbar behavior. *Coastal Engineering* 95: 35-50.

Falqués, A., Coco, G., Huntley, D.A., 2000. A mechanism for the generation of wave-driven rhythmic patterns in the surf zone. *Journal of Geophysical Research* 105, C10: 24071-24087.

Garnier, R., Dodd, N., Falqués, A., Calvete, D., 2009. A mechanism inhibiting rip channel formation for oblique waves. *Proceedings of Coastal Dynamics 2009*, No. 36.

Holland, K.T., Holman, R.A., Lippmann, T.C., Stanley, J., Plant, N.G., 1997. Practical use of video imagery in nearshore oceanographic field studies. *IEEE Journal of Oceanic Engineering* 22(1): 81-92.
Holman, R.A., Stanley, J., 2007. The history and technical capabilities of Argus. *Coastal Engineering* 54: 477-491.
Hsu, T., Elgar, S., Guza, R.T., 2006. Wave-induced sediment transport and onshore sandbar migration. Coastal Engineering 53: 817-824.
Lippmann, T.C., Holman, R.A., 1989. Quantification of sand bar morphology: a video technique based on wave dissipation. *Journal of Geophysical Research* 94, C1: 995-1011.
Lippmann, T.C., Holman, R.A., 1990. The spatial and temporal variability of sand bar morphology. *Journal of Geophysical Research* 95, C7: 11575-11590.
Ojeda, E., Guillén, J., Ribas, F., 2011. Dynamics of single-barred embayed beaches. *Marine Geology* 280: 76-90.
Rutten, J., Ruessink, B.G., Price, T.D., 2017. Observations on sandbar behaviour along a man-made curved coast. *Earth Surface Processes and Landforms*, doi:10.1002/esp.4158.
Sonu, C.J., 1973. Three-dimensional beach changes. *The Journal of Geology* 81: 42-64.
Splinter, K.D., Holman, R.A., Plant, N.G., 2011. A behavior-oriented dynamic model for sandbar migration and 2DH evolution. Journal of Geophysical Research 116: C01020, doi:10.1029/2010JC006382.
Stive, M.J.F., De Schipper, M.A., Luijendijk, A.P., Aarninkhof, A.G.J., Van Gelder-Maas, C., Van Thiel de Vries, J.S.M., De Vries, S., Henriquez, M., Marx, S., Ranasinghe, R., 2013. A new alternative to saving our beaches from sea-level rise: The Sand Engine. *Journal of Coastal Research* 290: 1001-1008.
Thiébot, J., Idier, D., Garnier, R., Falqués, A., Ruessink, B.G., 2012. The influence of wave direction on the morphological response of a double sandbar system. *Continental Shelf Research* 32: 71-85.
Thornton, E.B., MacMahan, J., Sallenger Jr., A.H., 2007. Rip currents, mega-cusps, and eroding dunes. *Marine Geology* 240: 151-167.
Van Enckevort, I.M.J., Ruessink, B.G., 2001. Effect of hydrodynamics and bathymetry on video estimates of nearshore sandbar position. *Journal of Geophysical Research* 106, C8: 16969-16979.
Van Enckevort, I.M.J., Ruessink, B.G., 2003. Video observations of nearshore bar behaviour. Part 1: alongshore uniform variability. *Continental Shelf Research* 23: 501-512.
Van Enckevort, I.M.J., Ruessink, B.G., Coco, G., Suzuki, K., Turner, I.L., Plant, N.G., Holman, R.A., 2004. Observations of nearshore crescentic sandbars. *Journal of Geophysical Research* 109: C06028, doi:10.1029/2003JC002214.
Wright, L.D., Short, A.D., 1984. Morphodynamic variability of surf zones and beaches: a synthesis. *Marine Geology* 56: 93-118.
Yu, J., Slinn, D.N., 2003. Effects of wave-current interaction on rip currents. Journal of Geophysical Research 108, C33088, doi:10.1029/2001JC001105.